JOURNAL OF MATERIALS SCIENCE 27 (1992) 2695–2704

# Behaviour of unidirectional and crossply ceramic matrix composites under quasi-static tensile loading

A. W. PRYCE, P. A. SMITH
*Department of Materials Science and Engineering, University of Surrey, Guildford, Surrey GU2 5XH, UK*

Experimental results are presented for the quasi-static tensile behaviour of unidirectional, $(0/90)_s$, $(0_2/90_4)_s$ and $(0/90)_{3s}$ silicon carbide fibre (Nicalon) reinforced calcium aluminosilicate glass–ceramic matrix laminates. The stress–strain behaviour and associated damage development is described in detail for each laminate. The damage development is quantified by counts of crack density (in both the longitudinal and transverse plies) and stiffness reduction as functions of applied strain. The damage initiation and growth (and its effect on residual properties) are discussed with reference to the Aveston–Cooper–Kelly (ACK) theory for unidirectional ply cracking and crossply laminate shear-lag (originally developed for polymer matrix composites) to describe the transverse ply cracking behaviour.

## 1. Introduction

For continuous-fibre ceramic matrix composites (CMC) to be used in engineering applications a knowledge of and capability to model their mechanical behaviour are obviously of great importance. There are already in the literature a number of models which consider the cracking behaviour of unidirectional fibre-reinforced brittle-matrix materials loaded parallel to the fibre direction [1–5]. To model transverse ply cracking in crossply (i.e. 0/90 type) ceramic composites it should be possible to make use of some of the existing models developed for polymer matrix composites. Experimental data in the literature enabling such models to be tested are limited, although there are a number of studies which describe and interpret the basic mechanical behaviour (e.g. [6–10]). In the present work we present experimental observations on unidirectional and a range of crossply CMCs and apply simple models to interpret the observed behaviour.

## 2. Material and lay-ups

The materials used in the present work were Nicalon (trademark of Nippon Carbon Co.) SiC fibre-reinforced calcium aluminosilicate glass–ceramic matrix laminates manufactured by hot-pressing prepreg. Basic properties are shown in Table I. The lay-ups supplied (courtesy of Rolls-Royce plc) were $(0)_{12}$, $(0/90)_s$, $(0_2/90_4)_s$ and $(0/90)_{3s}$. The nominal ply thickness was 0.18 mm, although this varied by about 10% from lay-up to lay-up. By dissolving the glass matrix using hydrofluoric acid and by image analysis, the fibre volume fraction was determined as 34%.

## 3. Experimental procedure

Tensile coupons 80 mm by 20 mm were cut from the laminates. Both edges of the coupons were polished carefully and, as can be seen from Fig. 1, a high grade of finish was obtained. Due to the weak nature of the fibre–matrix bond some damage to fibres in longitudinal plies was incurred, but this did not limit the assessment of matrix damage under subsequent mechanical loading. It was observed that the ply thicknesses, fibre diameter and fibre distribution vary considerably. Micro-porosity, in the form of void strings running parallel to the plies, could also be seen, particularly in the $(0_2/90_4)_s$ lay-up. Such voids presumably arise from air and volatiles being trapped between layers of prepreg during consolidation of the laminate.

Abraded and etched aluminium end-tags were bonded on to specimens for ease of gripping in wedge grips. Quasi-static tests were carried out using an Instron 1175 under displacement control at a crosshead speed of 0.05 mm $min^{-1}$. Longitudinal and transverse strains were measured using strain gauges so that the modulus and Poisson's ratio could be determined. Some specimens were loaded continuously to failure, giving initial tangent values of modulus and Poisson's ratio. Other specimens were used in "discontinuous tests" in which they were loaded to progressively higher strain levels in order to study damage development. These tests also enabled the progressive changes in stiffness properties with applied strain (and extent of damage) to be determined.

Direct observations of matrix cracking were made using optical and scanning electron microscopy (detecting back-scattered electrons) of the polished

0022–2461 

TABLE I Summary of main matrix, fibre and unidirectional lamina properties (for $V_f = 0.35$)

| | | |
|---|---|---|
| $E_f$ | Fibre modulus | 190 GPa |
| $\alpha_f$ | Fibre thermal expansion coefficient | $3.3 \times 10^{-6}$ K$^{-1}$ |
| $E_m$ | Matrix modulus | 90 GPa |
| $\alpha_m$ | Matrix thermal expansion coefficient | $4.6 \times 10^{-6}$ K$^{-1}$ |
| $E_1$ | Lamina modulus (parallel to fibres) | 128 GPa |
| $E_2$ | Lamina modulus (perpendicular to fibres) | 85–110 GPa[a] |
| $\nu_{12}$ | Lamina principal Poisson's ratio | 0.24 |
| $G_{23}$ | Lamina shear modulus (through-thickness) | 36 GPa[b] |
| $\alpha_1$ | Lamina expansion coefficient (parallel to fibres) | $4.3 \times 10^{-6}$ K$^{-1}$ |
| $\alpha_2$ | Lamina expansion coefficient (perpendicular to fibres) | $4.5 \times 10^{-6}$ K$^{-1}$ |

[a] Range of values estimated from (0/90) data using laminated plate theory.
[b] Estimated assuming 2–3 plane is isotropic and using $G_{23} = E_2/2(1 + \nu_{23})$, taking $\nu_{23} = 0.25$.

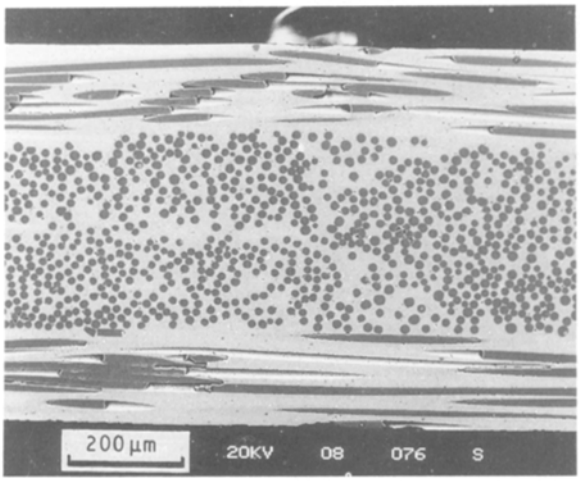


*Figure 1* Polished edge of a $(0/90)_s$ laminate.

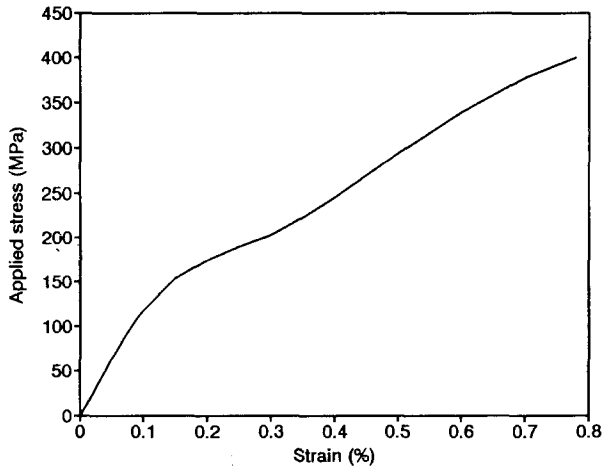


*Figure 2* Stress–strain curve for $(0)_{12}$ laminate.

coupon edges. As the residual opening of the cracks was very small, the coupons were placed in a straining stage after each load cycle and a small strain applied (< 0.05% for loading cycles > 0.06%) to open the cracks. When placed under the optical microscope, cracks were identified clearly at magnifications of 50 to 100 times. Crack densities were determined by counting the number of cracks in a gauge-length of about 15 mm except for the $(0_2/90_4)_s$ laminate, which has larger crack spacings in the $90_8$ plies, where a gauge-length of 50 mm was used.

## 4. Stress–strain behaviour and damage observations

### 4.1. Unidirectional laminate

The basic mechanical properties for the $(0)_{12}$ laminate are summarized in Table II. A typical stress–strain curve (Fig. 2) displays a well-defined "knee" at about 0.08% applied strain, which corresponds to the onset of matrix damage. This type of discontinuity and the general shape of the stress–strain curve have been observed for other CMC systems [6, 11]. The matrix damage is in the form of an array of cracks spanning the width and thickness of the laminate (Fig. 3), and the density of these cracks (i.e. the number of cracks per unit length) increases with increasing applied strain. The stress–strain curve becomes linear again at about 0.3%, suggesting that matrix cracking has saturated by this stage, and this was confirmed by crack counting (see next section). Final fracture of the laminate (involving fibre failure) occurs at a strain of about 0.8%.

TABLE II Initial moduli, moduli at failure, failure strengths and failure strains for $(0)_{12}$, $(0/90)_s$, $(0/90)_{3s}$ and $(0_2/90_4)_s$ laminates

| Laminate | Initial modulus[a] (GPa) | Poisson's ratio[a] | $\varepsilon_f$[b] (%) | $\sigma_u$[b] (MPa) | Final tangent modulus[b] (GPa) |
|---|---|---|---|---|---|
| $(0)_{12}$ | 128 ± 7 | 0.24 ± 0.03 | 0.78 | 400 | 39 |
| $(0/90)_s$ | 120 ± 20 | 0.24 ± 0.07 | 0.63 | 173 | 13 |
| $(0_2/90_4)_s$ | 101 ± 16 | 0.20 ± 0.03 | 0.65 | 107 | 8 |
| $(0/90)_{3s}$ | 110 ± 5 | 0.22 ± 0.05 | 0.63 | 146 | 12 |

[a] Mean of at least five specimens.
[b] One specimen only.

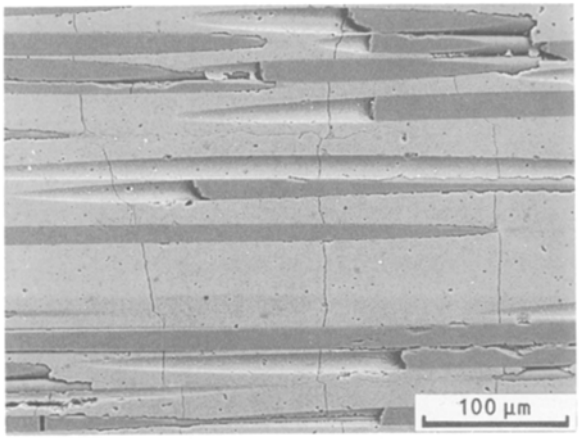


*Figure 3* Typical matrix cracking damage in $(0)_{12}$ laminate.

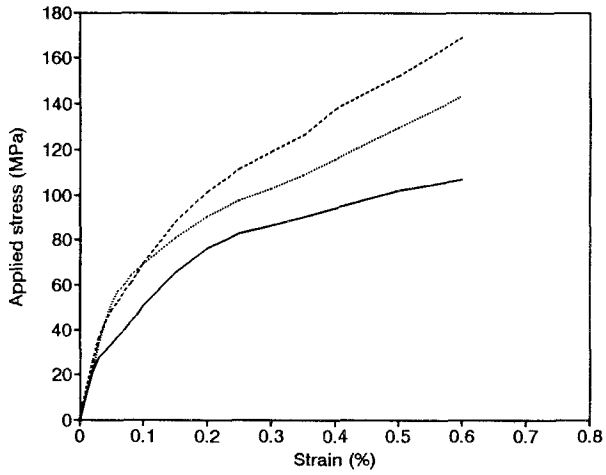


*Figure 4* Stress–strain curves for (---) $(0/90)_s$, (——) $(0_2/90_4)_s$ and ( . . . ) $(0/90)_{3s}$ laminates.

### 4.2. (0/90) laminates

Fig. 4 shows stress–strain curves for the various crossply laminates tested and Table II gives the basic mechanical properties. These laminates show an initial knee at between 0.02 and 0.04%, corresponding to matrix cracking in the 90° plies. From results for polymer matrix composites (or by applying simple strength/volume arguments) we would expect the crossply laminates with the thickest 90° plies to show the lowest knee. This is shown by the experimental results with the knee for the $(0_2/90_4)_s$ being at about 0.02% and those for the other laminates at greater than 0.03%. Cracking in the 90° plies continues with increasing strain (Fig. 5). At higher strains the matrix in the longitudinal plies also cracks. Sometimes the longitudinal ply cracks occur as a result of extension of existing 90° ply cracks into neighbouring 0° plies; they are also seen to form independently (Fig. 6). The crack density in both transverse and longitudinal plies continues to increase with increasing applied strain until eventually "saturation" (i.e. constant) crack spacings are observed. Final fracture of all the crossply laminates occurs at strains of 0.63–0.65%, compared to the value of 0.8% for the unidirectional material.

## 5. Crack density and modulus reduction data

The development of cracking and the associated degradation in laminate stiffness properties were studied in detail using discontinuous tests. As indicated earlier, the crack density was determined by counting the number of cracks visible on a polished edge within a known gauge length. Both edges of a coupon were examined periodically in order to check that the cracks counted extended across the ply width as well as the ply thickness. For specimens where the cracks spanned a ply in a direction more or less perpendicular to the applied load, crack counting was straightforward. However, for the thickest 90° plies (in the $(0_2/90_4)_s$ lay-up) the cracks were distinctly non-planar. In this case a systematic method of crack counting had to be used, as indicated in Fig. 7.

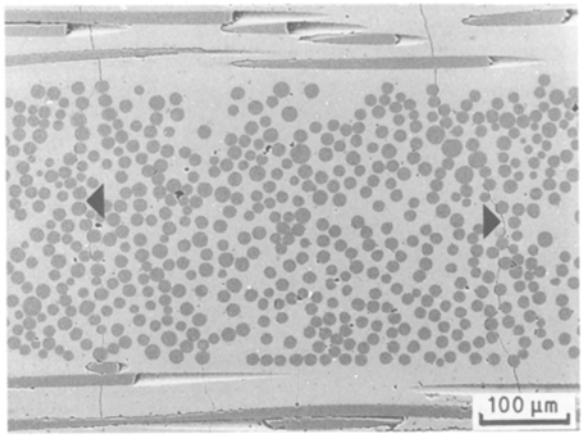


*Figure 5* Typical transverse ply cracking damage in $(0/90)_s$ laminate.

In previous work on polymer matrix composites [12] it was found, while performing discontinuous tests, that on reloading cracked specimens the stress–strain curves were linear until the stage where further cracking occurred, at which point the curves became non-linear. This was not so for the ceramic composites. Both unidirectional and crossply CMC lay-ups displayed non-linear stress–strain curves when previously cracked (see Fig. 8 for an illustration of this in the unidirectional material). This is a result of fibre–matrix sliding in the unidirectional material [1]. In the crossply material there is additionally the possibility of crack closure arising from frictional effects across the faces of any transverse ply cracks which are not perpendicular to the applied load; consequently these cracks will not open unless a certain stress is applied. Because of these effects the values of reduced moduli as a function of applied strain presented in this paper are secant values, measured at 0.05% applied strain for the unidirectional laminate and 0.02% for the crossply laminates.

### 5.1. Unidirectional laminate

Fig. 9 shows the crack density as a function of applied stress in the $(0)_{12}$ laminate while Fig. 10 shows the

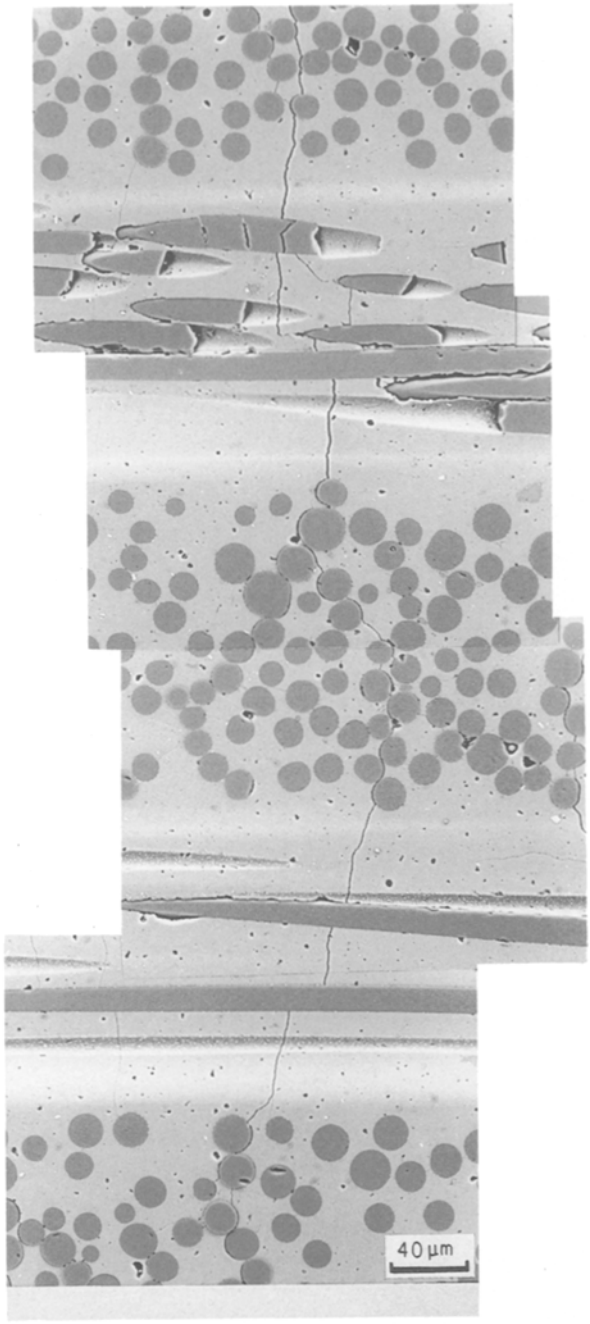


*Figure 6* Damage in $(0/90)_{3s}$ laminate showing 0° ply cracks, 90° cracks and cracks running across the entire thickness of the laminate.

same crack density data plotted as a function of applied strain, in which form they may be compared with the cracking data for the unidirectional plies of the various crossply laminates.

Fig. 11 shows the modulus as a function of applied strain. The overall stiffness reductions are large, reflecting the significant contribution made by the matrix to the laminate modulus. There may also be a contribution to the stiffness reduction in both the unidirectional and the crossplies from fibre breakage, and this will be investigated in future work.

## 5.2. (0/90) laminates

The results for the crossply laminates are presented in Fig. 10 and Figs 12 to 18. Considering first the $(0/90)_s$ laminate, Fig. 12 shows the crack density as a function

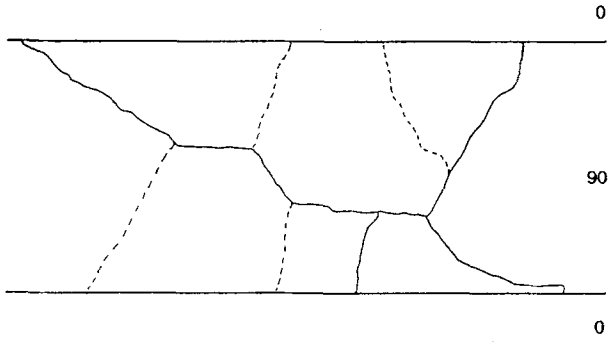


*Figure 7* Illustration of crack counting technique for $(0_2/90_4)_s$ laminate: crack count 1 = (——), crack count 2 = (——) + (– – –).

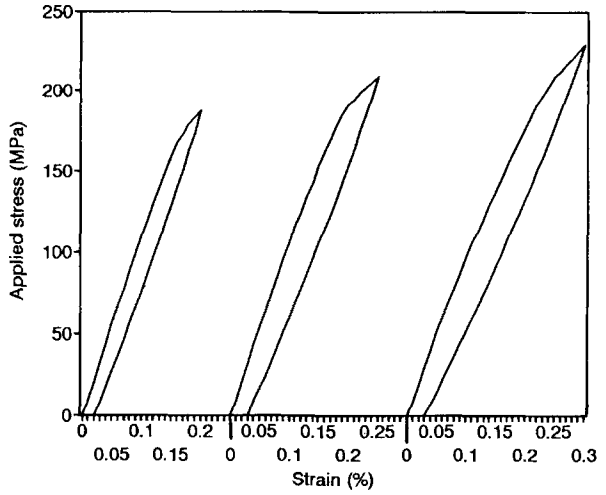


*Figure 8* Non-linearity of stress–strain behaviour in discontinuous tests on $(0)_{12}$ material.

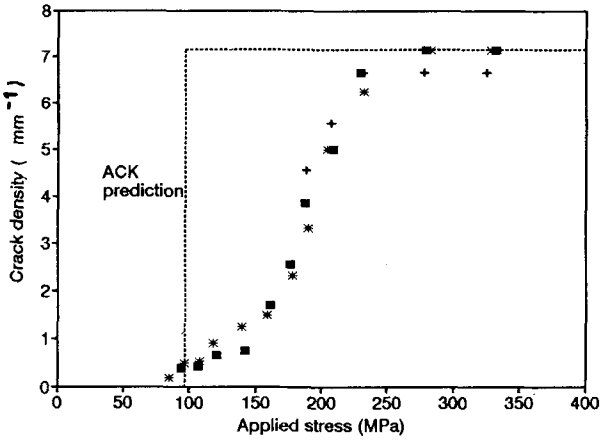


*Figure 9* Crack density as a function of applied stress in $(0)_{12}$ laminates and prediction of ACK model with $\tau = 10$ MPa, $2\gamma_m = 6\,J\,m^{-2}$.

of applied stress for the $90_2$ plies (in which form the data may be compared with a simple shear-lag model – see Section 6). Fig. 13 shows the same crack density data plotted as a function of applied strain; in this form the data may be compared with the results obtained from the $90_2$ plies in the $(0/90)_{3s}$ laminate. Fig. 14 shows the normalized stiffness of the $(0/90)_s$ laminate as a function of applied strain; note that this

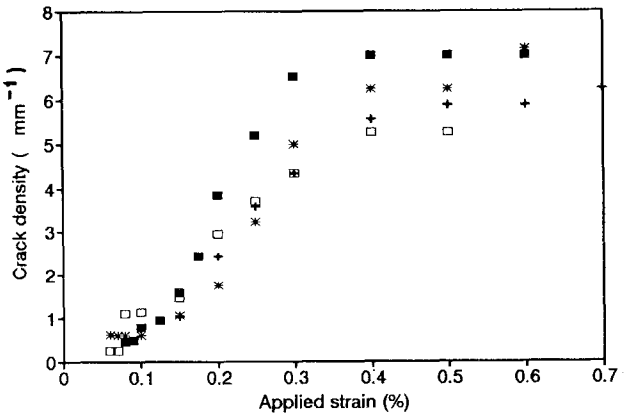


*Figure 10* Crack density as a function of applied strain in 0° plies of (■) $(0)_{12}$, ( + ) $(0/90)_s$, (*) $(0_2/90_4)_s$ and (□) $(0/90)_{3s}$ laminates.

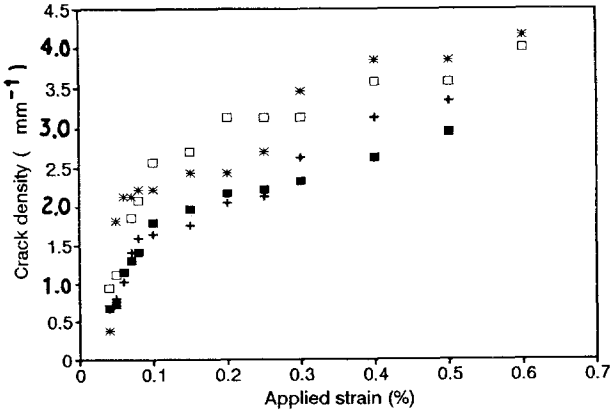


*Figure 13* Crack density as a function of applied strain for $90_2$ ply (0.35 mm thick) in (*, □) $(0/90)_s$ and (■, + ) $(0/90)_{3s}$ laminates.

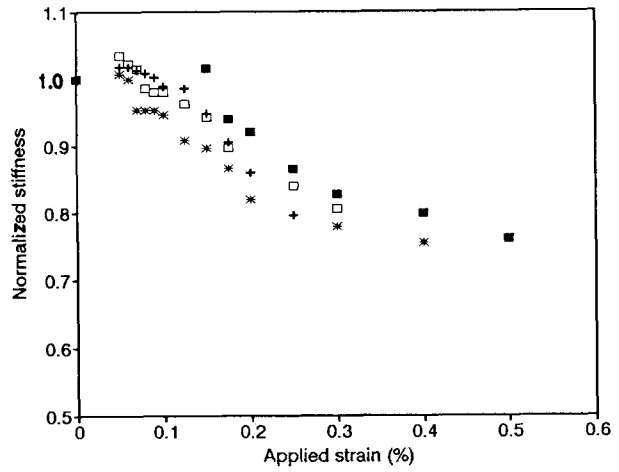


*Figure 11* Normalized stiffness as a function of applied strain in $(0)_{12}$ laminates.

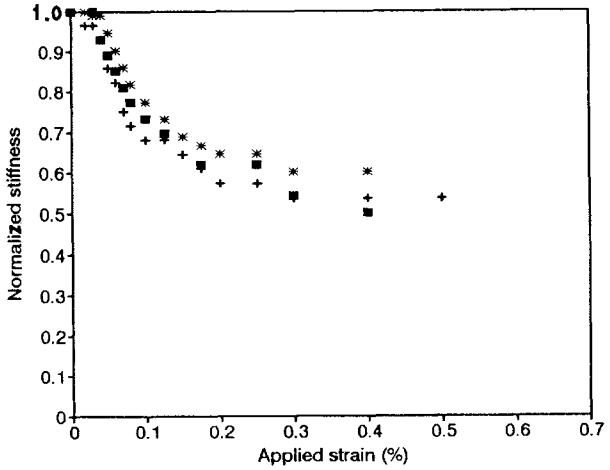


*Figure 14* Normalized stiffness as a function of applied strain in $(0/90)_s$ laminates.

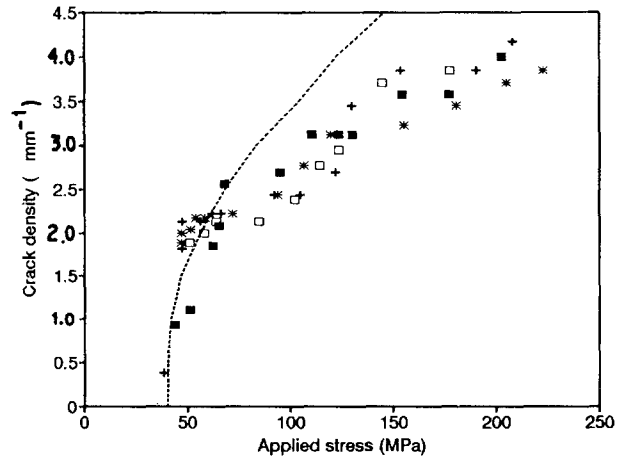


*Figure 12* Crack density as a function of applied stress for $90_2$ ply (0.35 mm thick) in $(0/90)_s$ laminate along with (– – –) prediction of simple shear-lag model (Equation 7).

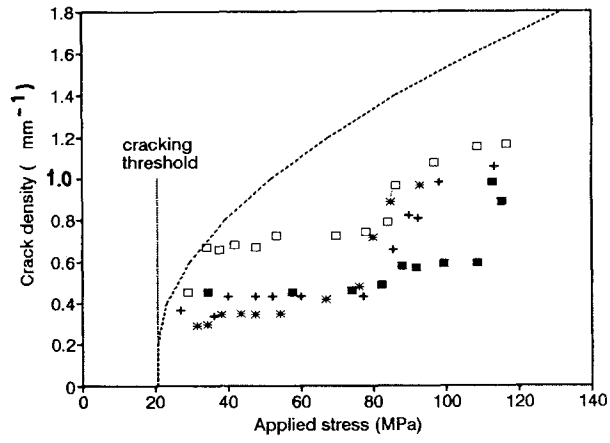


*Figure 15* Crack density as a function of applied stress for $90_8$ ply (1.39 mm thick) in $(0_2/90_4)_s$ laminate along with (– – –) prediction of simple shear-lag model (Equation 7).

stiffness reduction is a result of the combined effects of the $90_2$ ply cracking (Fig. 13) and the cracking of 0° plies (Fig. 10).

Fig. 15 shows the crack density in the $90_8$ plies of the $(0_2/90_4)_s$ as a function of applied stress (also compared with the shear-lag prediction – see Section 6) and Fig. 16 shows the same data plotted against applied strain. Fig. 17 shows the normalized stiffness as a function of applied strain, again reflecting longitudinal ply cracking (Fig. 10) as well as the $90_8$ cracking.

For the $(0/90)_{3s}$ laminate, Fig. 18 shows the crack density in the single 90° ply as a function of applied strain. Fig. 19 shows the normalized stiffness as a

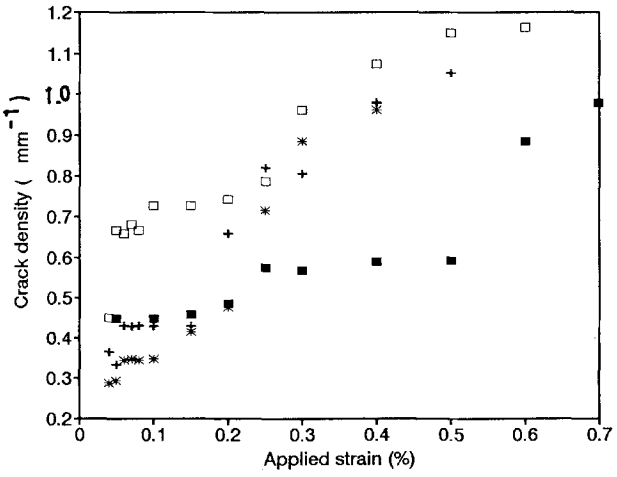


*Figure 16* Crack density as a function of applied strain for $90_8$ ply (1.39 mm thick) in $(0_2/90_4)_s$ laminate.

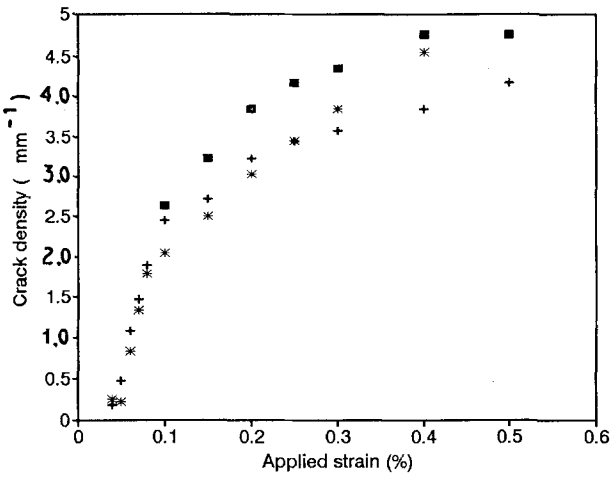


*Figure 18* Crack density as a function of applied strain for 90 ply (0.18 mm thick) in $(0/90)_{3s}$ laminate.

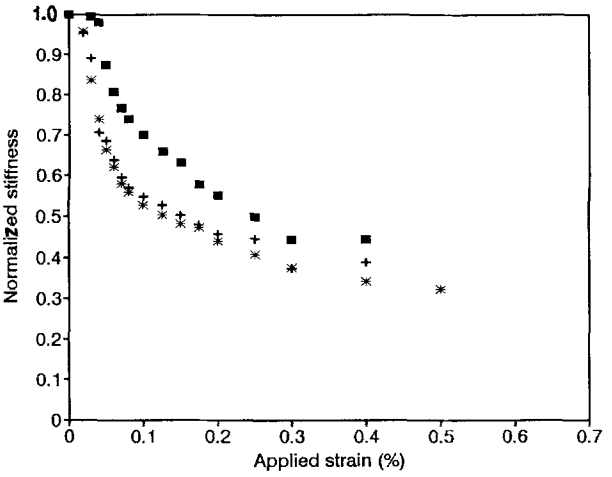


*Figure 17* Normalized stiffness as a function of applied strain in $(0_2/90_4)_s$ laminates.

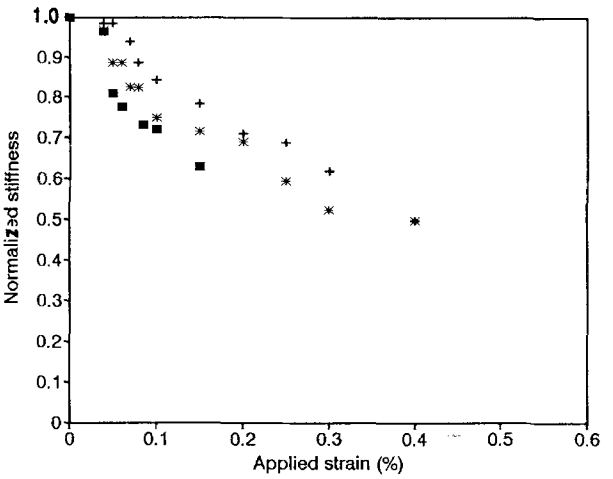


*Figure 19* Normalized stiffness as a function of applied strain in $(0/90)_{3s}$ laminates.

function of strain and represents the combined effects of the single 90° plies cracking (Fig. 18), the central $90_2$ cracking (Fig. 12) and the cracking of 0° plies (Fig. 10).

## 6. Discussion

### 6.1. Residual thermal stresses

In any modelling of the crack development in the laminates, it is necessary to take account of the stresses generated in the laminates as a result of mismatch in thermal expansion coefficients between the fibres and matrix, during cooling from the final processing stage. Suppliers' data give the principal coefficients of thermal expansion of unidirectional material, $\alpha_1$ and $\alpha_2$ (parallel and perpendicular to the fibre direction, respectively), as $4.3 \times 10^{-6}$ and $4.5 \times 10^{-6}\,K^{-1}$, while the values for the Nicalon fibre and CAS matrix are $\alpha_f = 3.2 \times 10^{-6}$ and $\alpha_m = 4.6 \times 10^{-6}$. For a temperature change of $-1200$ K (the material is "ceramed" at about 1500 K), the initial residual (tensile) thermal strain in the matrix of a unidirectional laminate parallel to the fibres is simply $(\alpha_m - \alpha_1)\Delta T$, i.e. $\sim 0.036\%$. For crossply laminates the thermal strain in the transverse ply (taken as being the matrix thermal strain) can be found using laminated plate theory (LPT, e.g. [13]) for any particular laminate lay-up and elastic constants. LPT gives the thermal strains in the transverse plies as 0.011% in the $(0/90)_s$ and $(0/90)_{3s}$ laminates and 0.009% in the $(0_2/90_4)_s$ laminate. The thermal strains in the matrix of the longitudinal plies in each laminate were estimated by inferring the effective composite laminate expansion coefficient from LPT and calculating the mismatch between this value and the expansion coefficient of the unrestrained matrix $\alpha_m$. Proceeding in this way, the thermal strains in the matrices of the 0° plies were estimated at 0.025% in the $(0/90)_s$ and $(0/90)_{3s}$ laminates and 0.022% in the $(0_2/90_4)_s$ laminate.

### 6.2. Initial elastic moduli of the laminates

The initial elastic moduli of the laminates are shown in Table II. The data show some variation which could be a result of cracks being present in the matrix as received, although nothing was seen on micrographs

to support this. The matrix makes a substantial contribution to the overall modulus of the laminate so that the moduli of the (0/90) laminates approach the modulus of the $(0)_{12}$ laminate. Although the modulus of a lamina perpendicular to the fibre direction ($E_2$) was not measured independently, it can be inferred from the crossply moduli by using laminated plate theory (or, to a good approximation, the rule of mixtures). Proceeding this way suggests that $E_2$ lies in the range 85–110 GPa, showing the CMC to be more isotropic than its polymer-matrix counterpart. The lower end of this range is inferred from the $(0_2/90_4)_s$ laminate, perhaps suggesting that the quality of the (thick) $90_8$ plies is not as good as that of the (thinner) transverse plies in the other laminates – certainly polished sections from the $(0_2/90_4)_s$ laminates show more porosity than any of the other lay-ups.

In all calculations for a particular lay-up (including the thermal stress calculations above) where a value of $E_2$ is needed, the inferred *in situ* value for that lay-up is used. Although the Poisson's ratios for the laminates show more scatter than the moduli (perhaps because a transverse gauge samples over a smaller volume than a longitudinal gauge), the trends are sensible. The value of $E_2$ inferred from the $(0/90)_s$ laminate is close to the $E_1$ value, hence the two principal Poisson's ratios of a 0° lamina ($\nu_{12}$ and $\nu_{21}$) are almost equal. Consequently we would expect the Poisson's ratio of the $(0/90)_s$ laminate to be very close to that of the $(0)_{12}$ laminate, and this was found experimentally. For the $(0/90)_{3s}$ laminate the inferred $E_2$ (and hence $\nu_{21}$) is lower than for the $(0/90)_s$ laminate and so the Poisson's ratio is lower for the $(0/90)_{3s}$ laminate. Finally, the $(0_2/90_4)_s$ laminate has the lowest $E_2$ value and also the greatest fraction of 90° plies; hence the Poisson's ratio value is the lowest of those of all the crossply laminates.

## 6.3. Cracking in unidirectional laminate

Many studies in the literature have attempted to model matrix cracking processes in unidirectional CMCs. The classic paper by Aveston *et al.* (ACK) [1] employs an overall energy balance to obtain an expression for the matrix cracking strain, $\varepsilon_{mu}$

$$\varepsilon_{mu} = \left(\frac{12\tau\gamma_m E_f V_f^2}{E_1 E_m^2 r V_m}\right)^{1/3} \quad (1)$$

where $E_m$, $E_f$ and $E_1$ are the modulus of the matrix, the fibre and the composite, respectively; $V_f$ is the volume fraction of fibre and $V_m$ ($= 1 - V_f$) is the volume fraction of the matrix; $r$ is the fibre radius. The quantity $\gamma_m$ is the fracture surface energy of the matrix and $\tau$ is the (assumed constant) interfacial shear stress between the fibre and matrix. Once a crack forms, then at the plane of that crack all the load on the composite is taken by the fibres. However, as a result of the interfacial shear stress, $\tau$, acting between the fibres and the matrix, the stress in the matrix increases linearly (from zero) with distance away from the crack plane. At a distance $x'$ from the crack the matrix failure strain is reached again. Consequently cracking continues with no further increase in applied load until there are approximately uniform cracks, spanning the width and thickness of the specimen, spaced between $x'$ and $2x'$ apart, where

$$x' = \frac{V_m}{V_f}\left(\frac{\sigma_{mu} r}{2\tau}\right) \quad (2)$$

and $\sigma_{mu} = E_m \varepsilon_{mu}$ is the fracture stress of the matrix.

Subsequent studies [2, 4] have considered the mechanics of crack growth in more detail and have shown that Equation 1 describes a lower bound for matrix cracking which is valid only if an initial flaw is present, of greater than a certain size (calculation shows this size to be of the order of a few fibre diameters).

We can use the above analyses to interpret the data of the present study. The crack density–applied stress data for the unidirectional laminate (Fig. 9) indicate that matrix cracking occurs over a range of applied stress. This is a result of the range of initial flaw sizes which lead to cracks (analysed by Marshall *et al.* [2] and McCartney [4]). The first cracks to go in (at about 0.08% strain applied, i.e. a stress of about 96 MPa) may occur due to the propagation of large pre-existing flaws, while those which occur at progressively higher strains could propagate from smaller pre-existing flaws. However, this is complicated by the non-uniform stress distribution in the matrix due to microstructural irregularities such as local fibre volume fraction and fibre diameter variations.

The final, or "saturation", crack spacing in the 0° laminates, $2s_f$, was 0.14 mm. Following Kimber and Keer [14]:

$$2s_f = 1.33x' \quad (3)$$

From Equations 1, 2 and 3 using the experimentally determined value of $\varepsilon_{mu}$ (0.12%, including thermal strain) and taking 8 μm as a representative value for the fibre radius, the inferred values of $\tau$ and $2\gamma_m$ are 10 MPa and 6 J m$^{-2}$, respectively. The value of $\tau$ is perhaps high while the value of $2\gamma_m$ is reasonable for a ceramic matrix [15]. These calculated values of $2\gamma_m$ and $\tau$ enable a "prediction" to be made for the data of Fig. 9, based on the ACK model. The plot shows clearly that the ACK model is an oversimplification as outlined above. The matrix cracks propagate over a range of applied stress. Although it is not attempted here, it should be possible to model the data of Fig. 9 by assuming that the 0° material has a statistical distribution of strengths along its length. Such a model would enable the low-strain part of the stress–strain curve, where matrix cracking is the dominant damage mechanism, to be described. At higher strains other damage mechanisms such as fibre breakage must become important.

## 6.4. Cracking in (0/90) laminates

First we consider the cracking thresholds of the 90° plies in the various laminates. These can be estimated in a consistent way by extrapolating the crack density–applied strain curves to the point where they

cross the strain axis, and the data found in this way were consistent with the strain at which there is the first discontinuity in the stress–strain curves from the continuous tests. Data for the $90_8$ plies crack density in the $(0_2/90_4)_s$ laminate could not be extrapolated reliably because the first strain interval in the discontinuous tests exceeded the cracking threshold, so for this laminate the threshold was taken from the first discontinuity in the stress–strain curves from continuous tests. For all laminates, the cracking strains obtained are then added to the calculated thermal strains to give the cracking thresholds shown in Table III.

These data confirm that the lowest cracking strain occurs in the laminate with the thickest transverse ply. In polymer composites the trend of increasing strain for first cracking in the transverse plies of crossply laminates of progressively smaller transverse ply thicknesses has been explained in two different ways. Using fracture mechanics arguments (e.g. [16–18]) it can be shown that for thin transverse plies the strain required to propagate a microcrack spanning the thickness of the ply across the width of the laminate is, to a first-order approximation, inversely proportional to the square root of the transverse ply thickness. This is the so-called "constrained cracking" situation. Alternatively, in a thick transverse ply the microcracks are smaller than the transverse ply thickness and the strength of the ply can be imagined to show a Weibull-type statistical distribution of strengths (corresponding to the stress levels at which the different size microcracks propagate) – in which case the thicker the ply the lower the expected mean strength (e.g. [19–21]). This is known as "unconstrained" transverse ply cracking and is the situation which we might expect to apply to CMCs.

To investigate this further, we use simple fracture mechanics methods to estimate the critical flaw size in the 90° plies of the crossply laminates in the following way. For a penny-shaped crack of radius $a$ in an infinite isotropic body, the stress intensity factor $K$ is given by [22]

$$K = 2\pi^{-1/2}\sigma a^{1/2} \tag{4}$$

Hence, for a transverse ply which cracks at a strain $\varepsilon_{fpf}$, by setting $K = K_{1C} = (E_2 2\gamma)^{1/2}$ where $\gamma$ is the fracture surface energy of the transverse ply and taking $\sigma = E_2\varepsilon_{fpf}$, the critical flaw size $a^*$ can be estimated from

$$a^* = \frac{\pi 2\gamma}{4E_2\varepsilon_{fpf}^2} \tag{5}$$

We can estimate $2\gamma$ very simply as $(1 - V_f)\,2\gamma_m$ (this is a mean toughness as a crack passes through a representative cross-section; if the bulk of the fracture path is at fibre–matrix interfaces we expect the toughness to be considerably lower). Using values for the different crossply laminates in Equation 5 suggests that the initial flaw diameter, $2a^*$, is about 0.23 mm in the $90_2$ plies of the $(0/90)_{3s}$ and $(0/90)_s$ laminates and 1.06 mm in the $90_8$ plies of the $(0_2/90_4)_s$ laminate. In each laminate the inferred flaw size is less than the transverse ply thickness, and the flaw size is larger in the laminate with the largest transverse ply volume. It is probable that the true flaw sizes are all smaller than calculated due to the value of $2\gamma$ used being too high. Given these small critical flaw sizes, it would appear that cross-ply ceramic matrix composite laminates will exhibit unconstrained cracking for practical ply thicknesses.

Transverse ply cracks increase in density with further loading beyond the initiation strain in a very similar manner to polymer matrix composites. If we assume that the plies of the composite remain bonded and that the response is elastic, then we can describe the stress distributions in a cracked (0/90) composite using shear-lag analysis (e.g. [18, 23, 24]). For a $(0/90)_s$ laminate of longitudinal ply thickness $b$ and transverse ply thickness $2d$ containing a regular array of transverse cracks spaced $2s$ apart, the longitudinal stress distribution in the transverse ply as a function of distance $y$ (measured along the length of the specimen from a coordinate origin midway between two cracks) is

$$\sigma_2 = \left(\sigma\frac{E_2}{E_0} + \sigma_2^T\right)\left(1 - \frac{\cosh\lambda y}{\cosh\lambda s}\right) \tag{6}$$

where $E_0$ is the rule-of-mixtures modulus of the laminate, equal to $(bE_1 + dE_2)/(b + d)$, $\sigma$ is the applied stress, $\sigma_2^T$ is the initial thermal stress in the transverse ply and

$$\lambda^2 = \frac{3G_{23}(b + d)E_0}{d^2 bE_1E_2} \tag{7}$$

TABLE III Summary of cracking thresholds (from extrapolating crack density–applied strain curves and adding the calculated thermal strain) and saturation crack spacings for laminates tested

| Laminate | Ply | Thickness (mm) | Threshold cracking strain (%) | Saturation crack spacing (mm) |
|---|---|---|---|---|
| $(0)_{12}$ | $0_{12}$ | 2.10 | 0.12 | 0.14 |
| $(0_2/90_4)_s$ | $0_2$ | 0.43 | 0.10 | 0.15 |
| $(0/90)_s$ | 0 | 0.16 | 0.14 | 0.16 |
| $(0/90)_{3s}$ | 0 | 0.17 | 0.08 | 0.18 |
| $(0_2/90_4)_s$ | $90_8$ | 1.39 | 0.03 | 0.9 |
| $(0/90)_s$ | $90_2$ | 0.35 | 0.05 | 0.25 |
| $(0/90)_{3s}$ | $90_2$ | 0.36 | 0.05 | 0.33 |
| $(0/90)_{3s}$ | 90 | 0.18 | 0.05 | 0.25 |

Following Garrett and Bailey [23], Equation 6 can be used to predict progressive matrix cracking in a very simplistic way by assuming that the next set of cracks form midway between existing cracks (i.e. at $y = 0$) when the stress at that point reaches the transverse ply strength, $\sigma_{2u}$, (assumed constant – which is not correct given that there will be a distribution of initial flaw sizes present). The necessary applied stress for further cracking, $\sigma'$, is then given by

$$\sigma' = \left(\frac{\sigma_{2u}}{[1 - (1/\cosh \lambda s)]} - \sigma_2^T\right) E_0/E_2 \quad (8)$$

The prediction of Equation 8 is compared with the experimental data for 90° cracking in the $(0/90)_s$ and $(0_2/90_4)_s$ laminates in Figs 12 and 15, respectively. Agreement with the trends of the data is reasonable. However, there are two main factors which need to be incorporated to improve this type of model. Firstly the statistical nature of the 90° failure processes needs to be incorporated (perhaps using an approach along the lines of that of Fukunaga *et al.* [20] for polymer composites). Secondly, at high strains the effect of the degradation of the stiffness of the constraining plies, $E_1$, as a result of their cracking must be considered.

Fig. 13 enables crack development in the $90_2$ plies of two different laminates as a function of applied strain to be compared. The behaviour is similar as might be expected, given that both plies demonstrate unconstrained cracking.

The "saturation" crack spacings for the 90° plies are summarized in Table III. For polymer matrix composites it is well established that "saturation" matrix cracking corresponds to an average crack spacing of the order of the ply thickness (e.g. [25]). From Table III it is clear that saturation crack spacing in the $90_8$ plies (0.9 mm) is greater than in the other plies and substantially less than their thickness (1.39 mm). The $90_2$ plies saturate at a crack spacing (0.25–0.33 mm) about equal to their thickness (0.35 mm) while the single 90 ply saturates at a spacing (0.25 mm) rather larger than the ply thickness (0.18 mm). Overall there is an effect of transverse ply thickness on saturation crack spacing, as would be expected given that the transverse ply thickness influences the rate at which stress is shed back from the 0° plies into the 90° plies, but the trend is not well defined for the thinner plies. It is interesting that the saturation crack spacings in the crossply CMCs (especially for the $90_8$ plies) are smaller (as a multiple of the ply thickness) than for their polymer matrix counterparts. An explanation may be that in crossply polymer composites a limiting factor is the shear stress that can be sustained by the resin at the 0–90 interface, which in turn limits the transfer of load back into the 90° plies at small crack spacings, making additional cracking less likely. In glass matrix CMCs the interface will remain elastic at much higher loads, efficiently transferring stress back into the 90° plies by shear, even at small crack spacings, making further cracking possible.

As the transverse ply crack and longitudinal ply crack arrays develop in the laminates the moduli fall dramatically, as shown by the secant plots of Figs 11, 14, 17 and 19 and the tangent data of Table II. Shear-lag relations such as Equation 5 enable expressions for the normalized stiffness as a function of transverse ply crack density to be written; however, such expressions would need to be modified to account for the effect of 0° plies cracking. The limiting value for the modulus of a laminate where the matrix is fully discounted is simply $V_{f0}V_fE_f$, where $V_{f0}$ is the volume fraction of 0° plies in the laminate. The tangent data of Table II are much lower than the discount value for all four laminates. There are two probable reasons for this: firstly fibre breakage will occur before failure, reducing the modulus below the matrix discount value; secondly, there will be permanent strains associated with the damage which will not affect the true elastic modulus but will have been included in a value measured from a continuous stress–strain curve.

It is interesting to compare the cracking behaviour of the unidirectional plies in the crossply laminates with the cracking behaviour of the unidirectional laminate. In general the strain at which cracks initiate is similar (Fig. 10 and Table III). However, in some specimens, notably of the $(0/90)_{3s}$, longitudinal cracks occurred at lower strains than in the unidirectional material; when this happened, the cracks seemed to arise from the propagation of 90° cracks into the constraining 0° plies. The "saturation" crack spacing in the 0° plies of all the laminates seems to tend to the same value, independent of the 0° ply thickness. This is consistent with the model of stress transfer used in the ACK shear-lag analysis, i.e. that each fibre interacts with a cylinder of matrix in which it is contained; consequently it is the fibre radius which is the dimension governing stress transfer between fibre and matrix (Equation 2) and the ply thickness has no influence.

## 7. Concluding remarks

The present work has identified and quantified matrix cracking in unidirectional and cross-ply Nicalon-reinforced CAS matrix laminates. The unidirectional material cracks at a strain of about 0.12%, and crack development on further straining is consistent with that seen by other workers and can be described approximately using the ACK model. A more complete description of the stress–crack-spacing behaviour could be obtained by using the models of McCartney [4] or Marshall *et al.* [2] to deduce the microcrack distribution which develops into fully formed cracks over the range of stresses. The progressive cracking of unidirectional plies in crossply laminates is reasonably similar to that seen in unidirectional laminates: there is a similar threshold strain and saturation spacing. Transverse ply cracking in the crossply laminates initiates at low strains (about 0.03–0.05%) and is unconstrained in that the critical flaw sizes are estimated to be much smaller than the ply thickness. A simple shear-lag model, which assumes elastic bonding between the plies, describes the trend of the crack multiplication with applied load but needs to be modified to account for (a) the statistical nature of the failure process and (b) the effect of the simultaneous cracking of the 0° plies.

## Acknowledgements

The authors would like to thank Rolls-Royce plc for financial support and Ms Clara Davies, Dr David Dawson and Dr David Clarke of Rolls-Royce (Derby) and our colleague Dr Julie Yeomans for many helpful discussions.

## References

1. J. AVESTON, G. A. COOPER and A. KELLY, in Proceedings of The National Physical Laboratory (IPC Science and Technology Press Ltd, 1971), Paper 2, pp. 15–25.
2. D. B. MARSHALL, B. N. COX and A. G. EVANS, *Acta Metall.* **33** (1985) 2013.
3. B. BUDIANSKY, J. W. HUTCHINSON and A. G. EVANS, *J. Mech. Phys. Solids* **34** (1986) 167.
4. L. N. McCARTNEY, *Proc. R. Soc.* **A409** (1987) 329.
5. A. G. EVANS and D. B. MARSHALL, *Acta Metall.* **37** (1989) 2567.
6. K. M. PREWO, *J. Mater. Sci.* **21** (1986) 3590.
7. O. SBAIZERO and A. G. EVANS, *J. Amer. Ceram. Soc.* **69** (1986) 481.
8. B. FORD, R. G. COOKE and S. NEWSAM, *Proc. Br. Ceram. Soc.* **39** (1987) 229.
9. A. SEERAT-UN-NABI and B. DERBY, in Proceedings of 9th Riso International Symposium on Metallurgy and Materials Science, 1988, edited by S. I. Andersen, H. Lillholt and O. B. Pedersen (Risø National Laboratory, Roskilde, Denmark) p. 463.
10. K. M. PREWO, B. JOHNSON and S. STARRETT, *J. Mater. Sci.* **24** (1989) 1373.
11. T. MAH, M. G. MENDIRATTA, A. P. KATZ, R. RUH and K. S. MAZDIYASNI, *J. Amer. Ceram. Soc.* **68** (1985) 248.
12. P. A. SMITH and J. R. WOOD, *Compos. Sci. Tech.* **38** (1990) 85.
13. R. M. JONES, "Mechanics of Composite Materials", (Scripta–McGraw-Hill, Washington, DC, 1975).
14. A. C. KIMBER and J. G. KEER, *J. Mater. Sci. Lett.* **1** (1982) 353.
15. H. C. CAO, E. BISCHOFF, O. SBAIZERO, M. RUHLE and A. G. EVANS, *J. Amer. Ceram. Soc.* **73** (1990) 1691.
16. A. PARVIZI, K. W. GARRETT and J. E. BAILEY, *J. Mater. Sci.* **13** (1978) 195.
17. S. L. OGIN and P. A. SMITH, *Scripta Metall.* **19** (1985) 779.
18. N. LAWS and G. J. DVORAK, *J. Compos. Mater.* **22** (1988) 900.
19. P. W. MANDERS, T-W. CHOU, F. R. JONES and J. R. ROCK, *J. Mater. Sci.* **18** (1983) 2876.
20. H. FUKUNAGA, T-W. CHOU, P. W. M. PETERS and K. SCHULTE, *J. Compos. Mater.* **18** (1984) 339.
21. P. W. M. PETERS, *ibid.* **18** (1984) 545.
22. J. F. KNOTT, "Fundamentals of Fracture Mechanics" (Butterworths, London, 1973).
23. K. W. GARRETT and J. E. BAILEY, *J. Mater. Sci.* **12** (1977) 157.
24. S. L. OGIN, P. A. SMITH and P. W. R. BEAUMONT, *Compos. Sci. Tech.* **22** (1985) 23.
25. J. E. MASTERS and K. L. REIFSNIDER, in "Damage in Composite Materials", ASTM STP 775 (1982) p. 40.

*Received 17 January*
*and accepted 7 June 1991*